[13] Minucci, M. A. S., Toro, P. G. P., Chanes, J. B., Jr., Ramos, A. G., Pereira, A. L., Nagamatsu, H. T., and Myrabo, L. N., "Investigation of a Laser-Supported Directed-Energy 'Air Spike' in Mach 6.2 Air Flow — Preliminary Results," AIAA Paper 2001-0641, Jan. 2001.

T. C. Lin
Associate Editor

Plume Interference Effects on Missile Bodies

S. Raghunathan,* H. D. Kim,† and E. Benard‡
Queen's University Belfast,
Belfast, Northern Ireland BT9 5AG, United Kingdom
and
P. Mallon§ and R. Harrison¶
Thales Defence, Ltd.,
Belfast, Northern Ireland BT6 9HB, United Kingdom

Nomenclature

C_p = pressure coefficient, $(p - p_\infty)/(\frac{1}{2}\rho_\infty V_\infty^2)$
M_∞ = freestream Mach number
P_c = total pressure at the combustion chamber
p = local pressure
p_a = freestream static pressure
V_∞ = freestream velocity
x = axial distance
ρ_∞ = freesteam density

Introduction

IN recent years, there has been considerable progress in propulsion technology for supersonic flight bodies. The development of missile powerplants that produce high thrust density (ratio of thrust to reference cross-sectional area) has introduced several missile aerodynamic problems. These include degradation of longitudinal stability, reduced control effectiveness, and induced yawing moments, largely due to the strong interaction between an underexpanded exhaust plume and the boundary layer along the missile body surface.[1–6]

The interaction between a supersonic freestream and plume on a missile body[2,3] is typified in Fig. 1. Jet expansion at the nozzle exit produces a deflection of the external freestream flow and generates a rise in pressure, partially communicated upstream through the viscous layer very close to the body surface. In supersonic external flows, this nearly always leads to a series of oblique compression waves. For large jet-to-freestream pressure ratios, the compression waves coalesce to form a strong shock wave, leading to boundary-layer separation forward of the base. The supersonic plume is generated by the interaction of an imperfectly expanded supersonic jet with its surrounding conditions and has a number of distinct flow regions with different characteristic features.

For large jet pressure ratios, as experienced in missile systems, the plume is often characterized by an inviscid barrel shock cell structure, with shear layers developing along the plume and Mach disks. Embedded zones of subsonic flow occur just behind the Mach disks, and slipstreams generate from the triple point of the Mach disk and the barrel shocks, whereas a significant portion of the plume mixing layer may be subsonic even for jets exhausting into supersonic external freestream. This is due to the plume-induced shock on the missile body.

The plume-induced shock can lead to plume-induced separation, involving interaction between the separated shear layers, the shock waves, and the boundary layer. It is essential to have a detailed understanding of these interactions for an effective design of tactical missiles, but such an understanding is lacking at present. This Note presents research investigations directed toward a better understanding of the complex flow features over a missile body.

Computational Analysis

Computational fluid dynamic (CFD) studies were performed for simple missile configurations, namely, a cone cylinder (Fig. 2) and an ogive cylinder, with and without the exhaust plume. The model had a length L of approximately 1000 mm (varied slightly for comparison with the wind-tunnel data) and diameter D of 40 mm. The ogive-cylinder cone length of the model l was 240 mm (Fig. 3).

A commercially available code, Fluent 5, that is the most capable of analyzing the complex compressible flows around the missile body was used. The code has the ability to predict the flowfields involving strong shock interactions with shear layers and boundary layers.

Fluent 5 uses a fully implicit finite volume method to solve either the Euler or the Navier–Stokes equations. For the viscous turbulent flow analysis, two-equation turbulent stress models, standard k–e and renormalized group (RNG) k–e, which were modified to take account for compressibility effect, are employed to close the governing equations.

In the present computations, structured grids were employed for the simple missile configuration. With respect to temporal discretization, an explicit multistage time-stepping scheme is used to discretize the time derivatives in the governing equations. Using a second-order-accurate scheme with fine computational grids in the vicinity of the shock and wake flow makes it feasible to capture the shock structure near the forebody, as well as the wake flow downstream of the afterbody, of the missile model. The computational effort of effectively capturing them was reduced in the present computations by using an adaptive finite volume grid algorithm.

A multigrid scheme was used to accelerate the convergence of the solution on a series of coarse grid levels. The net mass flux through the computational boundaries was investigated to determine if there was an applicable imbalance through the boundaries.

In the case of the computations of the plume interference, the computational domain strongly affects the solutions obtained. With a high plume pressure ratio, the computational boundary downstream should be extended sufficient to reduce the high pressure of the plume to atmospheric conditions. In the present computations, the domain was extended about $40L$ upstream from the missile model and about $120L$ downstream away from the missile body.

The pressure far-field boundary conditions were used to simulate freestream conditions at infinity, with the inlet and outlet boundaries providing the requisite flow conditions. In addition to the model wall and the symmetry boundary conditions, the pressure inlet along the upstream boundary, the pressure outlet along the downstream boundary, and the pressure far-field on the sidestream boundary can specify another set of boundary conditions.

In the current computations, freestream Mach number M_0 was varied in a range of low supersonic flow speeds. Freestream static pressure and temperatures were kept constant 101325.1 Pa and 288.15 K, respectively, as is typical in wind-tunnel test flows. These conditions result in Reynolds number based on the model length from 2.0×10^7 to 4.5×10^7. The plume pressure ratio, defined as the ratio P_c/p_a of total pressure P_c at the combustion chamber to freestream static pressure p_a, was varied in the range

Received 8 March 2001; revision received 15 August 2001; accepted for publication 7 December 2001.

*Professor and Head of School, School Aeronautical Engineering. Associate Fellow AIAA.
†Senior Visiting Fellow, School Aeronautical Engineering. Member AIAA.
‡Lecturer, School Aeronautical Engineering.
§Senior Team Manager, Aerodynamics.
¶Director of Engineering, Future Research.

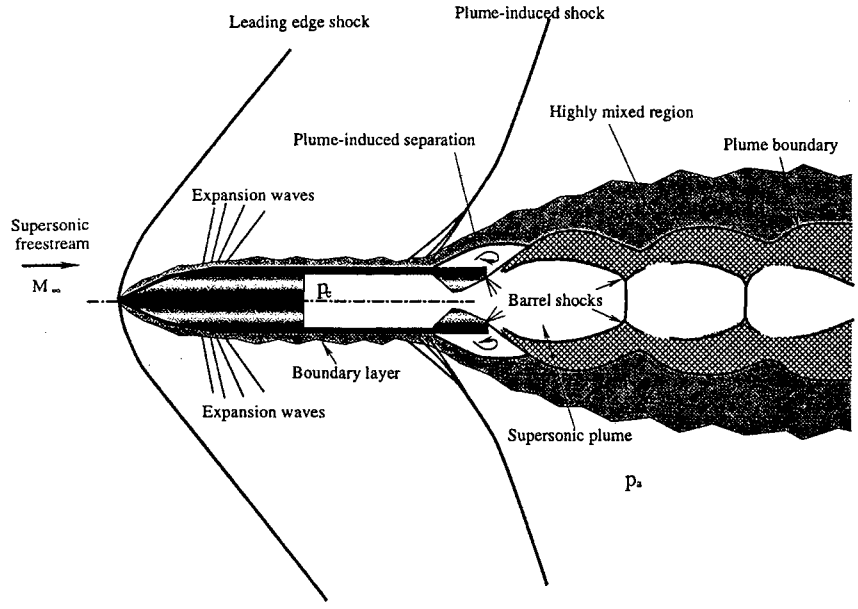

Fig. 1 Schematics of interaction between supersonic freestream and plume.

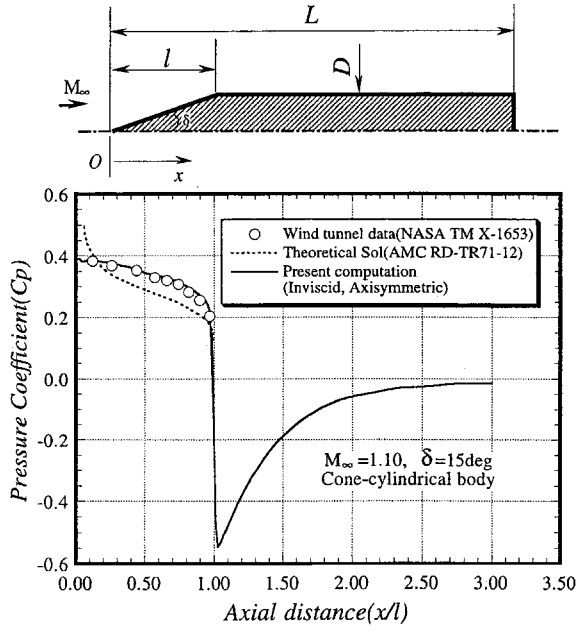

Fig. 2 Comparison of CFD results with experimental data: cone cylinder model.

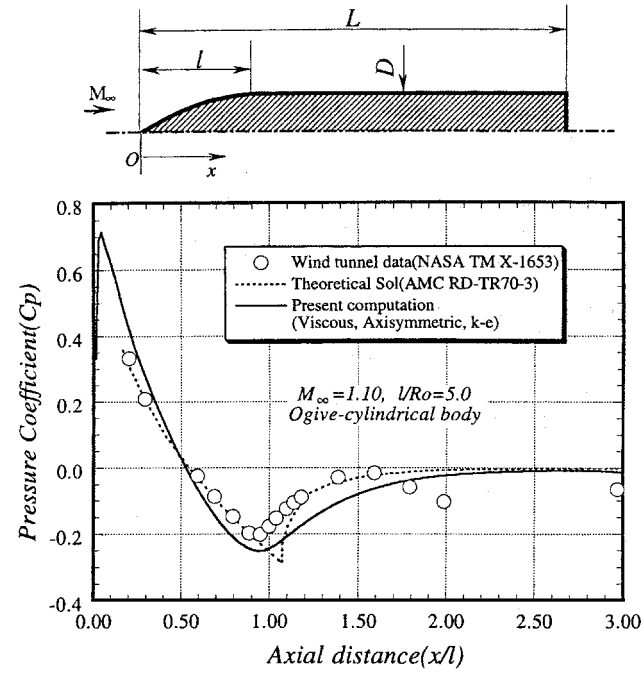

Fig. 3 Comparison of present computation with existing wind-tunnel data: ogive-cylindrical model.

of 1.5–2000. For simplicity, the total temperature at the combustion chamber was assumed the same as the freestream total temperature.

Results and Discussion

Results of the computations are shown in Figs. 2–5.

A result of computational analysis and comparison with experimental data for a cone-cylinder model at $M = 1.2$ and a large incidence is shown in Fig. 2. There are difficulties in computing flowfield at only Mach 1, where it can be seen that the agreement between the computational result and wind-tunnel data is very poor. In case of the small cone angles, the flow around the body is very sensitive to the disturbances due to the presence of the cone, and the entire flowfield in the present computational domain appeared highly unsteady. In spite of several tests, it was difficult to get grid-independent solutions for this particular case. This was not a problem for a larger cone angle. This may be associated with a stability problem appearing in a sonic flow past a very slender body. Agreement between CFD predictions and experiments for pressure distributions is good for a Mach number of 1.1 and larger cone angles of 15 deg.

For the ogive-cylinder body without the plume flow (Fig. 3) the flowfield is very sensitive to the ogive contour. Details of the contours used in the experiments were not available, and, therefore, the CFD predictions based on the contour chosen here can lead only to qualitative comparison with experiments. The CFD results agree well with the experiments for the shock position. Small differences in the results between the prediction and experiment are found due to the difference in geometry used.

For an ogive cone cylinder model with a plume, there are good agreements between CFD predictions and experimental data for pressure distributions on the ogive-cylinder body (Fig. 4) at transonic speeds and at zero incidence. Agreements are better at higher plume ratios. These results provide confidence in the use of CFD for predicting the flowfield of missiles with plume.

For a given freestream Mach number, there is a large effect of plume pressure ratios on the flow around the missile body (Fig. 5). The static pressures upstream of the shock on the body do not depend on the plume pressure ratio. With an increase in plume

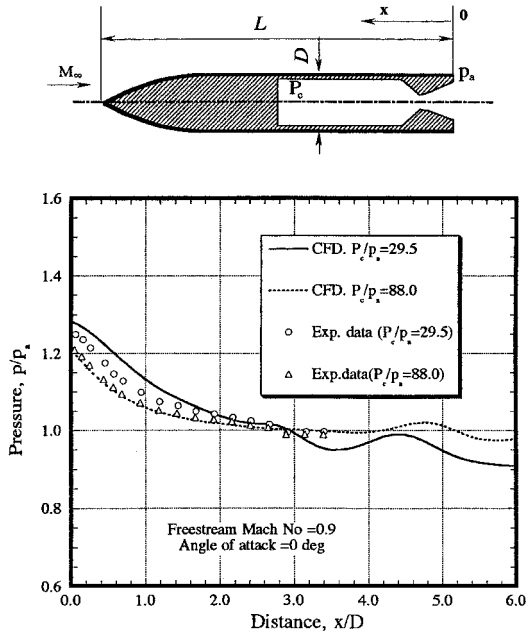

Fig. 4 Comparison of CFD results and wind-tunnel data: tangent-ogive cone cylinder model with plume.

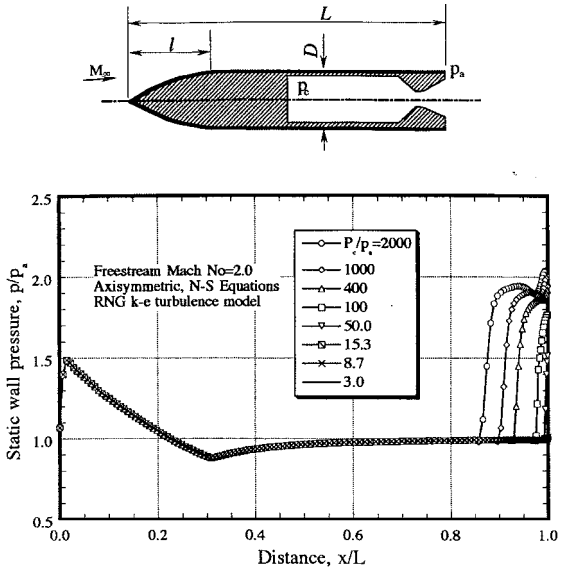

Fig. 5 Static pressure distributions along the body surface ($M_0 = 2.0$): tangent-ogive cone cylinder model with plume.

pressure ratio, the plume-induced shock wave moves upstream. Therefore, it may be reasonable to conclude that an increase in the plume pressure ratio has a similar effect to that of a decrease in the freestream Mach number. Note that there exists a large region of separation at the foot of the plume-induced shock on the body.

Conclusions

The conclusions from these analyses are as follows: Several features of plume flow and its interference effects on aft-mounted control surfaces can be clearly identified by CFD analysis. Plume pressure ratio has a significant effect on the plume in reference. For a given plume pressure ratio, an increase in Mach number resulted in an increase in shock strength and rearward motion of the shock on the tail fin.

References

[1]Dryer, N., and North, W. J., "Preliminary Analysis of the Effect of Flow Separation Due to Rocket Jet Pluming on Aircraft Dynamic Stability During Atmospheric Exit," NASA Memo 4-22-59E, 1959.

[2]Alpinieri, T. C., Jr., and Adams, R. H., "Flow Separation due to Jet Pluming," *AIAA Journal*, Vol. 4, No. 10, 1966, pp. 1865, 1866.

[3]McGhee, R. J., "Jet-Plume-Induced Flow Separation on a Lifting Entry Body at Mach Numbers from 4.00 to 6.00," NASA TM X-1997, April 1970.

[4]Klineberg, J., Kubota, T., and Lees, L., "Theory of Exhaust-Plume/Bounday-Layer Interactions at Supersonic Speeds," *AIAA Journal*, Vol. 10, No. 5, 1972, pp. 581–588.

[5]Boger, R. C., Rosenbaum, H., and Reeves, B. L., "Flowfield Interactions Induced by Underexpanded Exhaust Plumes," *AIAA Journal*, Vol. 10, No. 3, 1972, pp. 300–306.

[6]Burt, J. R., Jr., "An Investigation of the Effectiveness of Several Devices in Simulating a Rocket Plume at Free Stream Mach Numbers of 0.9 to 1.2," U.S. Army Missile Command, RD-TR-71-22, Redstone Arsenal, AL, Sept. 1971.

R. M. Cummings
Associate Editor

Implementation of an Aerodynamic Toolbox in a Reentry Flight Simulator

A. Guidi,* Q. P. Chu,† J. A. Mulder,‡ and J. Buursink§
Delft University of Technology,
2629 HS Delft, The Netherlands

Nomenclature

C_A	=	axial-force coefficient
C_{Ab}	=	axial-force coefficient of the base pressure
C_f	=	friction coefficient
C_M	=	moment coefficient
C_N	=	normal force coefficient
C_{Nb}	=	normal force coefficient of the base pressure
C_p	=	pressure coefficient
C_{pb}	=	pressure coefficient of the base pressure
$C_{p\,max}$	=	pressure coefficient in stagnation point
c	=	reference length, m
F	=	force, N
F_x	=	force in x direction, N
F_y	=	force in y direction, N
i	=	unit vector in x direction
j	=	unit vector in y direction
L	=	reference length, m
M	=	Mach number
M	=	moment, Nm
n	=	vector perpendicular to the surface
$P_{stagnation\ max}$	=	maximum stagnation point pressure, Pa
p	=	pressure, Pa
p_{stag}	=	stagnation point pressure, Pa
p_∞	=	freestream pressure, Pa
R, r	=	radius, m
R_B	=	base radius, m
R_N	=	nose radius, m

Received 10 October 2001; revision received 10 April 2002; accepted for publication 23 September 2002.

*Aerospace Engineer; currently Aerospace Engineer, University of Naples "Federico II," Via A. D'Isernia, 59, 80122 Naples, Italy; oceanomare@inwind.it. Member AIAA.

†Assistant Professor, Control and Simulation Division, Delft Aerospace, Kluyverweg, 1. Senior Member AIAA.

‡Professor, Chairman of the Control and Simulation Division, Delft Aerospace, Kluyverweg, 1. Senior Member AIAA.

§Research Assistant, Delft Aerospace, Kluyverweg, 1. Member AIAA.